

Slow and steady wins the race: Fractionated near-infrared treatment empowered by graphene-enhanced 3D scaffolds for precision oncology

Giordano Perini^{a,b,1}, Valentina Palmieri^{b,c,1}, Andrea Papait^{b,d}, Alberto Augello^b, Daniela Fioretti^e, Sandra Iurescia^e, Monica Rinaldi^e, Elsa Vertua^f, Antonietta Silini^f, Riccardo Torelli^g, Angela Carlino^h, Teresa Musarraⁱ, Maurizio Sanguinetti^{g,j}, Ornella Parolini^{b,d}, Marco De Spirito^{a,b}, Massimiliano Papi^{a,b,*}

^a Dipartimento di Neuroscienze, Università Cattolica del Sacro Cuore, Largo Francesco Vito 1, 00168, Rome, Italy

^b Fondazione Policlinico Universitario A. Gemelli IRCCS, 00168, Rome, Italy

^c Istituto dei Sistemi Complessi, CNR, Via dei Taurini 19, 00185, Rome, Italy

^d Dipartimento di Scienze della Vita e Salute Pubblica, Università Cattolica del Sacro Cuore, 00168, Rome, Italy

^e Istituto di Farmacologia Traslazionale (IFT), Dipartimento di Scienze Biomediche, CNR, 00133, Rome, Italy

^f Centro di Ricerca Eugenia Menni, Fondazione Poliambulanza Istituto Ospedaliero, 25124, Brescia, Italy

^g Dipartimento di Scienze di Laboratorio e Infettivologiche, Fondazione Policlinico Universitario A. Gemelli IRCCS, 00168, Rome, Italy

^h Dipartimento di Medicina e Chirurgia, Università Internazionale San Camillo per la Salute e le Scienze Mediche (Unicamillus), 00131, Rome, Italy

ⁱ Unità di Patologia Testa e Collo, Polmone e Endocrinologia, Fondazione Policlinico Universitario Agostino Gemelli IRCCS, 00168, Rome, Italy

^j Dipartimento di Scienze Biotecnologiche di Base, Cliniche Intensivologiche e Perioperatorie-Sezione di Microbiologia, Università Cattolica del Sacro Cuore, Rome, Italy

ARTICLE INFO

Keywords:

Graphene oxide
3D printed scaffolds
Cancer therapy
Near-infrared radiation
Photodynamic therapy

ABSTRACT

Surgically addressing tumors poses a challenge, requiring a tailored, multidisciplinary approach for each patient based on the unique aspects of their case. Innovative therapeutic regimens combined to reliable reconstructive methods can contribute to an extended patient's life expectancy. This study presents a detailed comparative investigation of near-infrared therapy protocols, examining the impact of non-fractionated and fractionated irradiation regimens on cancer treatment. The therapy is based on the implantation of graphene oxide/poly (lactic-co-glycolic acid) three-dimensional printed scaffolds, exploring their versatile applications in oncology by the examination of pro-inflammatory cytokine secretion, immune response, and in vitro and in vivo tumor therapy. The investigation into cell death patterns (apoptosis vs necrosis) underlines the pivotal role of protocol selection underscoring the critical influence of treatment duration on cell fate, establishing a crucial parameter in therapeutic decision-making. In vivo experiments corroborated the profound impact of protocol selection on tumor response. The fractionated regimen emerged as the standout performer, achieving a substantial reduction in tumor size over time, surpassing the efficacy of the non-fractionated approach. Additionally, the fractionated regimen exhibited efficacy also in targeting tumors in proximity but not in direct contact to the scaffolds. Our results address a critical gap in current research, highlighting the absence of a standardized protocol for optimizing the outcome of photodynamic therapy. The findings underscore the importance of personalized treatment strategies in achieving optimal therapeutic efficacy for precision cancer therapy.

1. Introduction

The search for innovative strategies to address the complex nature of cancer has led to significant advancements in the realm of biomaterials and tissue engineering [1,2]. In recent years, significant advancements have been made in scaffold design and fabrication techniques, allowing

for precise control over scaffold architecture, composition, and bioactivity [3–5]. Among these advancements, the integration of three-dimensional (3D) printing technology with novel biomaterials has emerged as a cutting-edge approach with immense potential [6–8]. These scaffolds serve as templates to guide tissue regeneration, enabling the formation of functional and organized tissues [9].

* Corresponding author. Dipartimento di Neuroscienze, Università Cattolica del Sacro Cuore, Largo Francesco Vito 1, 00168, Rome, Italy.

E-mail address: massimiliano.papi@unicatt.it (M. Papi).

¹ Authors contributed equally to this work.

Graphene oxide (GO), a derivative of graphene, has gathered substantial attention due to its remarkable features and versatile applications in the biomedical field [10–13]. GO is a well-known photosensitizing agent, that can absorb near-infrared (NIR) light and convert it efficiently into heat [14–16]. Moreover, GO demonstrates excellent capability to generate reactive oxygen species (ROS) upon light irradiation, promoting selective destruction of tumor cells while minimizing damage to healthy tissues [17–20]. In combination with biocompatible polymers, such as poly(lactic-co-glycolic acid) (PLGA), GO can be used to create 3D printed scaffolds, offering a powerful platform for both cancer treatment and, at the same time, tissue regeneration [21,22]. PLGA is renowned for its outstanding biocompatibility, making it well-suited for biomedical applications. Its use in scaffold fabrication is particularly advantageous, as PLGA can be easily processed, facilitating the integration of nanomaterials such as GO [23, 24]. Furthermore, the selection of PLGA is strategic in the field of scaffolds and prosthetics due to its tunable properties. Indeed, the copolymer composition of PLGA, combining lactic acid (PL) and glycolic acid (GA), allows for precise modulation of mechanical properties by adjusting PL/GA ratio [24]. Increasing the GA content, for instance, enhances the scaffold's strength, while augmenting the PL component improves flexibility. This tunability is crucial for addressing specific clinical needs, such as the type of tissue reconstruction, and accommodating anatomical requirements [23]. Moreover, PLGA provides the added advantage of customizable degradation and resorption kinetics, according to clinical demands [25]. Increasing the percentage of GA in the PLGA composition results in scaffolds that degrade more rapidly. Conversely, adjusting the ratio in favor of PL extends the degradation timeline, providing flexibility in designing scaffolds tailored to different clinical scenarios.

The unique characteristics of GO, including its excellent biocompatibility, high surface area, drug-loading capacity and tunable photothermal/photodynamic properties, make it an ideal candidate for multifunctional therapeutics [26–29]. In recent years, photothermal therapy (PTT) and photodynamic therapy (PDT) have emerged as promising strategies for cancer treatment, harnessing the localized generation of heat and ROS in response to external light irradiation in the presence of photosensitizing agents [30,31]. PDT involves the administration of photosensitizing agents, which, upon exposure to light of a specific wavelength, undergo activation. This activation induces the generation of ROS, resulting in localized damage to cancer cells. Several clinical applications of PDT have demonstrated its efficacy across different malignancies. Dermatological studies showcase PDT as a successful method for treating skin cancers, including basal cell carcinoma and actinic keratosis [32]. The precision of PDT allows for targeted treatment of cancerous lesions while minimizing damage to healthy tissue. In gastrointestinal cancers, particularly esophageal and early-stage gastric cancers, PDT has proven effective. The localized effects of PDT, facilitated by direct light delivery during endoscopic procedures, enhance the treatment precision. Lung cancer, both in early and advanced stages, has been a focus for PDT interventions [33]. PDT for bladder cancer involves intravesical administration of photosensitizing agents directly into the bladder offers a targeted approach for treating superficial tumors [34]. The adaptability of PDT across various cancer types and anatomical locations reflects its potential as a non-invasive and targeted therapeutic approach. As we explore the integration of advanced nanomaterials like graphene or MXenes into PTT/PDT strategies, a new frontier emerges. These nanomaterials exhibit exceptional properties, including high photothermal conversion efficiency. In simpler terms, they efficiently convert IR light, which penetrates tissues deeply, into heat.

To date, optimizing the appropriate NIR radiation dose for PTT/PDT remains largely unexplored, with extremely limited prior research focusing on identifying the most effective and efficient administration of such therapies for anticancer treatment [35,36]. Therefore, in this study, we aim to bridge this critical gap by conducting a comprehensive

investigation comparing two distinct strategies: a single radiation session lasting 9 min, non-fractionated (NF) versus a fractionated approach comprising three radiation sessions of 3 min each, administered consecutively over three consecutive days (t1, t2, and t3). We irradiated 3D printed PLGA scaffolds having different concentrations of GO with an infrared laser at different power densities both in vitro and in vivo to provide a comprehensive understanding of the therapeutic outcomes. In the in vitro assessments, we focused on crucial parameters such as cell viability, production of ROS, expression of cytokines, and the type of cell death induced by each PTT/PDT strategy. To evaluate the translational potential of our findings, we established a murine breast cancer model wherein mice were inoculated with cancer cells and subsequently implanted with the PLGA-GO scaffolds. Even after a short-term application of the NIR treatment, noticeable regression of the tumor was observed. We observed distinct variations in the therapeutic responses elicited by the two PTT/PDT strategies. Notably, fractionated (t3) demonstrated a superior efficacy both in vitro and in vivo, suggesting its potential as a more robust approach for anticancer treatment, providing valuable insights into the comparative efficacy of NF and t3 strategies in the context of PTT/PDT.

The results highlight the potential of this approach for targeted cancer cell eradication and reducing immune toxicity. The comparative evaluation of two different doses of NIR radiation provides valuable insights into the efficacy of different treatment protocols and can help to identify the most effective approach for anticancer treatment, paving the way towards clinical translation to the emerging field of PTT/PDT-based therapies.

2. Materials and methods

2.1. GO characterization, 3D printing and characterization of PLGA-GO scaffolds

GO (Graphenea) was characterized by atomic force microscopy (AFM), dynamic light scattering (DLS), Raman spectroscopy, X-ray photoelectron spectroscopy (XPS). Raman spectra of GO were acquired at room temperature using backscattering geometry on an inVia Renishaw micro-Raman spectrometer, which was equipped with an air-cooled CCD detector and super-Notch filters. The excitation source employed was an Ar⁺ ion laser with a wavelength (laser) of 514 nm, coupled to a Leica DLML microscope featuring a 20× objective. The spectral resolution achieved was 2 cm⁻¹, and calibration was performed utilizing the 520.5 cm⁻¹ line of a silicon wafer. For XPS, GO was drop-casted on a Si(100) surface. Measurements were conducted utilizing a customized Omicron NanoTechnology MXPS system. The system was outfitted with a monochromatic Al K α X-ray source (Omicron XM-1000), operating the anode at 14 kV and 16 mA, with a photon energy (h ν) of 1486.7 eV. DLS and Zeta potential analysis were conducted using a Zetasizer Nano S from Malvern Instruments, Malvern, UK, equipped with a 4 mW He–Ne laser (633 nm). Measurements were undertaken at a constant angle of 173° relative to the incident beam.

To obtain PLGA-GO composites, PLGA flakes (Rimless Industry) and GO (Graphenea) were mixed keeping a fixed amount of PLGA and varying GO from 0 to 5% w/w in dichloromethan (Carlo Erba). The mixture of PLGA and GO was put in agitation overnight, then air dried. The produced film was cut into small pieces, then it was transferred to a thermoplastic printhead (Cellink), having a heating capacity of up to 250 °C. The structure of scaffolds was designed using modeled 3D computer graphics and computer-aided design (CAD) software Rhinoceros software (Robert McNeel & Associates). PLGA-GO scaffolds were printed via an extrusion-based technique at a printhead temperature of 185 °C and a printed temperature of 65 °C. The extrusion pressure was set at 40 kPa, with a preflow of 20 ms and a speed of 22 mm/s. GO from Graphenea was characterized by AFM with a NanoWizard II (JPK Instruments). Scaffolds were microscopically characterized through AFM as well. For this purpose, samples were imaged by using silicon

cantilevers with high aspect-ratio conical silicon tips (CSC36 Mikro-Masch) characterized by an end radius of about 10 nm, a half conical angle of 20°, and a spring constant of 0.6 N/m. Small scan areas (3 × 3 μm for GO, 10 × 10 μm for scaffolds) were imaged. Surface roughness parameters were extrapolated for scaffolds with the JPK Data Processing software (JPK Instruments). Scanning electron microscopy (SEM) images were acquired with SEM Supra 25 (Zeiss). All the samples were sputter-coated with gold. Fourier-transform infrared spectroscopy (FTIR) was conducted with an ALPHA II compact FTIR spectrometer (Bruker), to evaluate the correct surface chemical composition of scaffolds. Samples were directly laid upon the crystal and the spectra were recorded in the wave number range of 4000–550 cm⁻¹.

2.2. Near-infrared laser

A NIR laser (LaserEver) focused at 808 nm was used to perform PDT on cells. First, the laser was characterized by evaluating the laser power at every current intensity by using a power meter. The spot of the laser had a diameter of 0.8 cm. The power density was evaluated by normalizing the laser power to the area of the spot. To test the photo-thermal conversion of PLGA-GO scaffolds, constructs having different concentrations of GO -ranging from 0 to 5% w/w- were used. Scaffolds were put in a 48-well (Corning) and covered with 300 μL of culture medium. Then, they were irradiated at different power densities, depending on the concentration of GO, to achieve the same final temperature. Scaffolds having GO at 0.5% were irradiated with a current of 1.1 A, corresponding to a power density of 0.9 W/cm². Scaffolds of PLGA-GO 1% were irradiated with a current of 1.08 A, corresponding to a power density of 0.85 W/cm². Scaffolds of PLGA-GO 2% were irradiated with 1.06 A, corresponding to 0.8 W/cm². Finally, scaffolds of PLGA-GO 5% were irradiated at 1.02 A, corresponding to 0.75 W/cm². Scaffolds without GO were irradiated with the same power density of GO 0.5%, since no thermal increase was observed due to the absence of photoabsorbers. Thermal increase was monitored using a thermal camera (Optris) focused on the well. Two distinct PTT/PDT strategies were used in this work: a single radiation of 9 min (not fractioned, NF) and 3 radiations of 3 min each, one per day (t1, t2 and t3).

2.3. Evaluation of the photodynamic effect

To verify the direct photodynamic conversion effect of the scaffolds, the ROS-ID detection kit (Enzo Life Sciences) was employed. The kit allows for the assessment of comparative levels of total ROS, while also enabling the determination of superoxide production. The kit comprises two major components: the Oxidative Stress Detection Reagent (Green) for ROS detection and the Superoxide Detection Reagent (Orange). The green probe reacts directly with a broad spectrum of reactive species, yielding a green fluorescent product indicative of cellular production of various ROS types. In contrast, the orange probe, a cell-permeable superoxide detection dye, specifically reacts with superoxide, generating an orange fluorescent product. In our study, we irradiated PLGA-GO scaffolds in 48-well plates (Corning) for 3 min or 9 min, to reproduce the experimental conditions of the two NIR regimens. Scaffold were immersed in the Detection Solution during the timecourse of the experiment. After NIR, the 3D-printed constructs were incubated at 37 °C, 5% CO₂ for 1 h. Then, fluorescence intensity in the supernatant was recorded with a Cytation 3 Cell Imaging Multi-Mode Reader (Biotek) by exciting at 490 nm and reading the emission at 525 nm (green probe) and by exciting at 550 nm and reading the emission at 620 nm (orange probe).

2.4. Cell culture

A549 human lung adenocarcinoma cells, 4T1 and 4T1-luc2 mouse mammary and the RAW 264.7 murine macrophage cell line were purchased from the American Type Culture Collection (ATCC; CRL-

2539TM, CRL-2539™, CRL-2539-LUC2, TIB-71™). A549 cells were maintained in Dulbecco's modified Eagle's medium DMEM medium-high glucose (D6429, Merck KGaA-Sigma Aldrich, Darmstadt, Germany) supplemented with 10% fetal bovine serum (FBS, Gibco™ 10270106, Thermo Fisher Scientific Inc.), 2 % penicillin-streptomycin (10,000 U/ml, Gibco™ 15140122, Thermo Fisher Scientific Inc.). 4T1 and 4T1 luc2 cells were maintained in RPMI 1640 Medium-ATCC modification (A1049101, Thermo Fisher Scientific Inc) supplemented with 10 % FBS (Gibco™ 10270106, Thermo Fisher Scientific Inc.), and 2 % penicillin-streptomycin (10,000 U/ml, Gibco™ 15140122, Thermo Fisher Scientific Inc.). 4T1-Luc2 cells are a luciferase-expressing cell line derived from parental line CRL-2539 by transduction with lentiviral vector encoding firefly luciferase gene (luc2). RAW 264.7 cells were maintained in DMEM (D6429, Merck KGaA-Sigma Aldrich, Darmstadt, Germany) supplemented with 10% FBS (Gibco™ 10270106, Thermo Fisher Scientific Inc.), 2 % penicillin-streptomycin (10,000 U/ml, Gibco™ 15140122, Thermo Fisher Scientific Inc.). Cells were kept in T75 flasks (Corning) at 37 °C, 5% CO₂ for further treatments. Human peripheral blood mononuclear cells (PBMCs) were obtained from heparinized whole blood samples using density gradient centrifugation (Histopaque 1077, Sigma-Aldrich).

2.5. Assay protocol to measure viability

WST-1(4-(3-(4-iodophenyl)-2-(4-nitrophenyl)-2H-5-tetrazolio)-1,3-benzene-disulfonate (ROCHE/CELLPRO-RO) colorimetric assay was carried out to determine the effects of NIR laser irradiation (808 nm) on cell proliferation at the above indicated condition. The assay was performed by 48-well plates, with seeding of 4T1 (5 × 10³ cells/well), A549 (1 × 10⁴ cells/well), RAW264.7 (3 × 10⁴ cells/well) cells on PLGA, PLGA-GO1% and PLGA-GO2% scaffolds. After each NIR application, cells were cultured for additional 24 h s and 30 μL per well of WST-1 solution were added to the culture medium and incubated for 2 h at 37 °C and 5% CO₂. Absorbance was subsequently determined using Cytation 3 Cell Imaging Multi-Mode Reader (Biotek) applying the wavelengths 450 nm for measurements and 650 nm for reference. All experiments were conducted in two wells for each condition and replicated at least three times. Cell proliferation was calculated by comparing the absorbance values of the samples after background subtraction. Cell viability was expressed as the percentage of cells seeded on PLGA. Cell viability of human PBMCs was assessed by staining PBMC harvested from the different culture conditions and by staining cells with E-Fluor 780 (ThermoFisher) to exclude dead cells. Stained cells were then acquired at FACS Symphony A3 within 1 h and results analyzed using Flowjo 10.7v (BD Biosciences).

2.6. ROS production

The production of ROS was evaluated to address the photodynamic effect of PLGA-GO scaffolds on cells. For the detection of ROS, the fluorinated derivative of 2',7'-di-chlorofluorescein (H₂DCFDA) was employed. This probe is nonfluorescent until the acetate groups are removed by intracellular esterases and oxidation occurs within cells. Thus, oxidation can be detected by monitoring the increase in the fluorescence intensity. Cells were seeded on 48-well plates (Corning), having PLGA-GO scaffolds on the bottom of each well, at a seeding density of 3 × 10⁵ cells/well. Plates were then incubated at 37 °C, 5% CO₂. After incubation, scaffolds having different concentrations of GO, ranging from 0 to 5% w/w were irradiated with an 808 nm infrared laser at different power densities to induce the same thermal increase. The two different therapeutic approaches previously described were used: NF and t3. After the treatment, the medium was replaced with PBS containing 10 μM H₂DCFDA. Cells were incubated for 30 min at 37 °C in 5 % CO₂. PBS containing H₂DCFDA was then removed, and cells were resuspended in complete medium. The fluorescence intensity of H₂DCFDA was recorded by using a Cytation 3 Cell Imaging Multi-Mode

Reader using an excitation wavelength of 495 nm and recording the emission at 528 nm. To correctly quantify the production of ROS after the treatment, results were normalized by the number of viable cells and expressed as folds change with respect to cells seeded on PLGA.

2.7. ELISA assay on cells supernatant

RAW264.7, 4T1 and A549 cell lines were seeded on PLGA, PLGA-GO 1% and PLGA-GO 2% scaffold in a 48-well plate at 3×10^4 , 5×10^3 and 1×10^4 cells/well, respectively. NIR laser irradiation (808 nm) was conducted on cell proliferation at the above indicated condition and supernatants were collected after each NIR application centrifuged at 1200 rpm for 5 min and stored at -80°C until use. Tumor necrosis factor- α (TNF- α), interleukin-6 (IL-6) and interleukin-8 (IL-8) release was measured in 4T1 and A549 culture medium using mouse or human ELISA development kits (PeproTech® EC Ltd., UK), respectively, according to the manufacturer's instructions. For mouse IL-8 detection was used macrophage inflammatory protein-2 (MIP-2) ELISA kit as it is the mouse functional IL-8 homologue. RAW264.7 supernatants were tested for mouse TNF- α (MABTECH, Sweden) IL-6 (Invitrogen, MA, USA), and IL-1 β (MyBioSource Inc., San Diego, CA). Supernatants were diluted 1:2 and recombinant standards were serially diluted according to the manufacturers' instructions in diluent solution and added to 96-well plates. Interleukins binding were detected by chromogen 2,2'-azino-bis(3-ethylbenzothiazoline-6-sulphonic acid (ABTS) or 3,3',5,5'-Tetramethylbenzidine (TMB) incubation, and color development was monitored at 405 nm or 450 nm, respectively, according to the manufacturers' instructions. The concentration of cytokines in the samples was determined from the standard curve.

2.8. ELISA assay on mouse serum

Sera diluted 1:2 were used for the detection of interleukin-6 (IL-6), tumor necrosis factor- α (TNF- α), and macrophage inflammatory protein 2 (MIP-2) using mouse ELISA development kits (PeproTech® EC Ltd., UK) according to the manufacturer's instructions as already described above. Interleukins binding were detected by chromogen 2,2'-azino-bis(3-ethylbenzothiazoline-6-sulphonic acid (ABTS) and color development was monitored at 405 nm.

2.9. Pattern of cell death assessed by WST-1 assay after NIR treatment

4T1 and A549 cells (5×10^3 and 1×10^4 cells/well) were seeded on PLGA-GO 2% scaffold and cultured in a 48-well plate. After 24 h, Caspase- or RIPK1-inhibitors (Z-VAD-FMK, Promega WI, USA; RIP1 inhibitor II, 7-Cl-O-Nec-1, Calbiochem, Merck KGaA Darmstadt, Germany) were added into the wells at final concentrations of 20 μM , or PBS as control, and NIR laser irradiation were conducted after 1 h. Each inhibitor was added to cancer cells before each NIR irradiation (three times in the t3 regimen and once in the NF regimen). The culture medium was refreshed each day during the t3 experiment, and the inhibitor was newly added to restore the required 20 μM concentration. 24 hrs after NIR irradiation, the WST-1 reagent was added for another 2 h and the resulting amount of formazan dye was analyzed by spectrophotometry at 450 nm.

2.10. In vivo antitumor therapy and tumor evaluation

All animal care and experimentation were conducted in compliance with the guidelines of the European Union Directive 2010/63 and the Italian Law D.Lgs. 26/2014 and with the approval of the Institutional Animal Experimentation Ethics Committee of 'Università Cattolica del Sacro Cuore (Rome, Italy) and the Italian Health Ministry registered under No. 223/2022-PR. Animal studies are reported in compliance with the ARRIVE guidelines. All possible efforts were made to minimize animal suffering and to reduce the number of animals used per condition

by calculating the necessary sample size before performing the experiments.

The animals were maintained at $22 \pm 2^\circ\text{C}$ under a 12 h–12 h light/dark cycle with 50–60% humidity for at least one week prior to the experiment.

Eight/nine-week-old female BALB/c mice, weighing $19,13 \pm 0,93$ g were subcutaneously injected into the backs with 50 μl of 4T1-luc2 cells suspension (2×10^6 cells/ml) to establish the ectopic breast cancer model. 4T1-Luc2 cells express luciferase through lentiviral vector encoding firefly luciferase gene (luc2) under control of EF-1 alpha promoter.

One week post tumor challenge, four groups were randomly established (n = 4): Tumor group (T), without adding any scaffolds or NIR, Tumor and Scaffold group (TS), tumor, scaffold and the Not Fractioned single NIR radiation treatment (NF), tumor, scaffold and the fractioned t1, t2, t3 (t3).

Animals were fully anesthetized by intraperitoneal injection 10 ml/kg of a solution composed by ketamine hydrochloride (8 mg/ml, Ketavet 100, MSD Animal Health S.r.l., Italy) and xylazine (0.7 mg/ml, Rompun 20, Bayer S.p.A., Germany). Buprenorphine (0.1 mg/kg, diluted to 0.015 mg/ml) was administered subcutaneously prior to recovery from anesthesia.

A small skin incision was carefully made at the edge of the tumor and the scaffolds were implanted beneath the tumor tissues. The skin was sutured with 6-0 suture string (Assut Europe, Italy) and groups NF and t3 were exposed, still under anesthesia, to the NIR laser at 0.8 W/cm^2 for 9 min or 3 min respectively, and the temperatures of tumor surface were recorded by a thermal camera (Optris) in real time during the treatment. Group t3 received the 3 min irradiation the next two days, also, under isoflurane anesthesia (2% isoflurane).

Tumor bioluminescence was evaluated to monitor tumor growth by Optical Imaging IVIS® System every 7 days starting from NIR treatment, named day 0, while animals were under isoflurane anesthesia. Images were acquired 10 min after intraperitoneal injection of D-Luciferin (25 mg/ml - 150 mg/kg). The first NIR treatment day was regarded as day 0. From day -7, mice weight was measured at each time point to verify animal health conditions.

Mice were sacrificed by cervical dislocation under general anesthesia 2 weeks after day 0, tumor tissues were soaked in 4% neutral buffered formalin, embedded in paraffin, sectioned into slices and stained with hematoxylin-eosin (H&E) in sequence and finally evaluated under light microscopy (Leica). Five tissue slices were selected from each sample, and then five visions were measured from each slice randomly. Blood samples were collected postmortem by cardiac puncture and, after 15–30 min at room temperature, centrifuged at $1000\text{--}2000 \times g$ for 10 min in a refrigerated centrifuge. The resulting sera were transferred into a clean polypropylene and stored at -80°C .

2.11. Analysis of PBMC proliferation

The collection of human peripheral blood mononuclear cells (PBMC) from healthy donors for research purposes was approved by the local ethical committee "Comitato Etico Provinciale di Brescia," Italy (NP 3968, July 2, 2020). PBMCs (1×10^5 /well in a 96-well plate) were activated with 125 ng/mL (final concentration) of anti-CD3 monoclonal antibody (Orthoclone OKT3, Janssen-Cilag, Cologno Monzese, Italy). Activated PBMCs (PBMC + anti-CD3) were grown for 3 days in RPMI 1640 medium (Cambrex) supplemented with 10% heat-inactivated FBS, 2 mM L-glutamine and P/S in the presence of PLGA scaffold or a scaffold of PLGA-GO at different concentrations (0.5, 1, 2, 5%), exposed or not to two different regimens of hypothermia induced by either NF or t3 with infrared laser. Activated PBMCs stimulated with infrared laser regimens in absence of scaffolds were used as controls in all experiments. All conditions were performed in triplicate. PBMC proliferation was assessed by incorporation of 5-ethynyl-2'-deoxyuridine (EdU) as previously described. Briefly, 10 μM EdU (Life Technologies) was added to

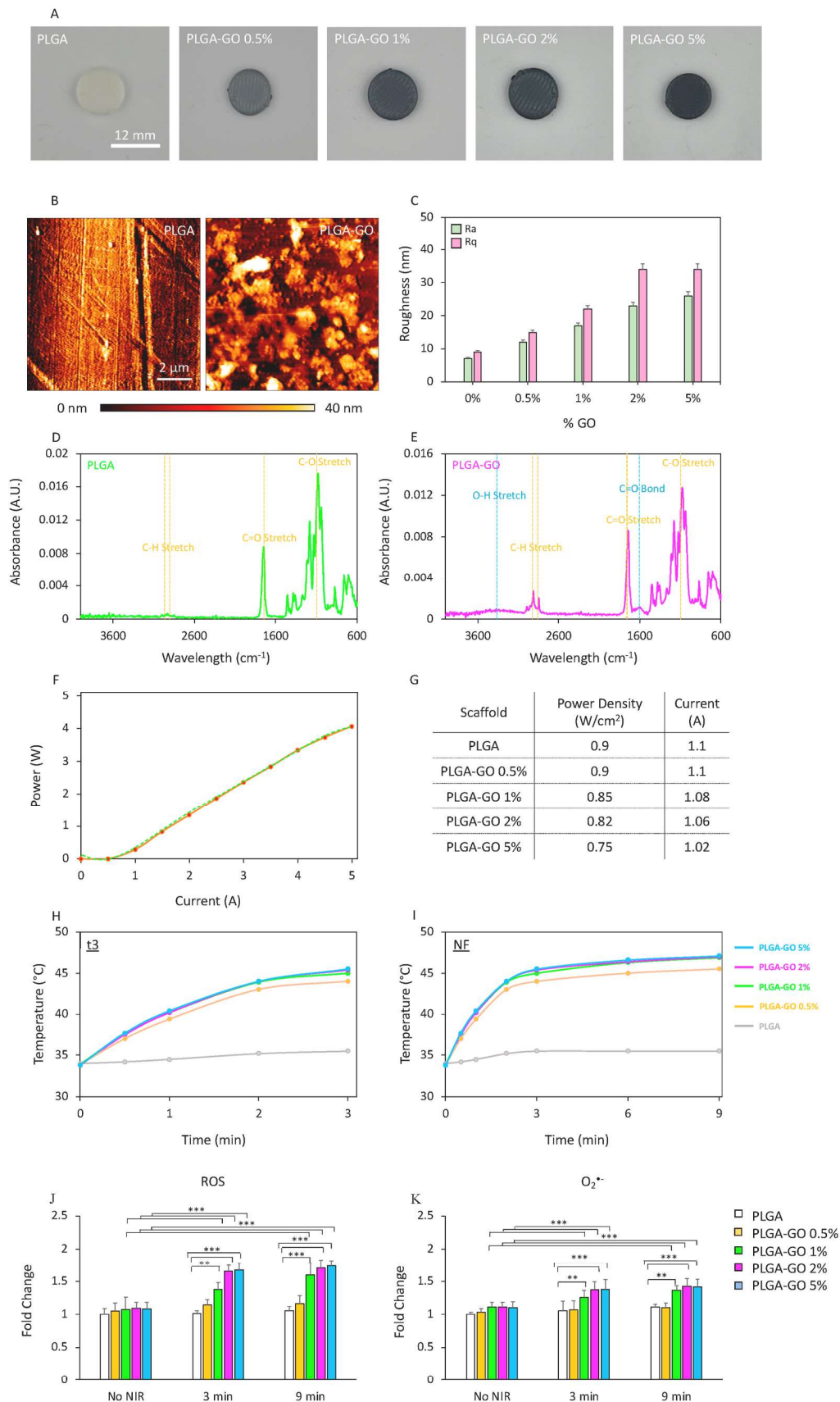


Fig. 1. Characterization of PLGA-GO scaffolds. **A)** Pictures of 3D printed PLGA-GO scaffolds having different concentrations of GO. **B)** AFM representative images of PLGA and PLGA-GO 2% scaffolds. **C)** Surface roughness of 3D printed scaffolds. **D-E)** FTIR spectra of PLGA and PLGA-GO scaffolds. **F)** Characterization of the 808 nm laser. **G)** NIR radiation specifications for the 3D printed materials. **H-I)** Temperature increase in a timespan of 3 min (t3) and 9 min (NF) for PLGA-GO scaffolds. **J-K)** Production of ROS induced by irradiating scaffolds without cells for 3 or 9 min ***p > 0.01 and ****p > 0.001 ANOVA and Turkey post-hoc test.

PBMCs at day 3 post-stimulation. After 16–18 h, cells were harvested and EdU incorporation was assessed by adding 2.5 μM 3-azido-7-hydroxycoumarin (Jena Biosciences) in a buffer solution (100 mM Tris-HCl pH 8.0, 10 mM L-ascorbic acid, 2 mM CuSO_4) at RT for 30 min. Cells were acquired with a FACS Symphony A3 (BD Biosciences), and the percentage of EdU-positive proliferating cells was analyzed with Flowjo v10.7. Cells were also stained with E-Fluor 780 (ThermoFisher) to exclude dead cells.

2.12. Phenotype of CD4^+ T helper (Th) and T regulatory (Treg) subsets

T helper (Th1, Th2, and Th17) and Treg subpopulations were identified by flow cytometry analysis for the expression of specific cell surface markers and transcription factors. After being co-cultured for 5 days with or without PLGA scaffold alone or with GO (0.5, 1, 2, 5%), activated PBMCs were harvested and centrifuged at 300 g for 5 min. The viable dye E-Fluor 780 from ThermoFisher was used to eliminate dead cells. CD3 (clone UCHT1), CD4 (clone VIT-4), CD45RA (clone HI100), CD196 (clone 11A9), CD183 (clone 1C6/CXCR3), CD25 (clone M-A25) all purchased from BD biosciences and CD194 (clone REA279) from Miltenyi. After fixation and permeabilization with BD Cytotfix/Cytoperm (BD Biosciences), intracellular staining for the transcription factor FoxP3 was carried out by incubating cells with anti-FoxP3 antibody (clone R16-715, BD Biosciences) 4 °C for 30 min in the dark. FACS Symphony A3 (BD Biosciences) was used to acquire the samples, and Flowjo 10.7v (BD Biosciences) was used to analyze the results. Th subsets and Treg were identified by the following gating strategy: first, $\text{CD4}^+\text{CD45RA}^-$ negative cells were gated to identify T effector cells, then Th subsets were identified as follows: Th1 as $\text{CD196}^-\text{CD183}^+$, Th17/Th1 as $\text{CD196}^+\text{CD183}^+$, Th2 as $\text{CD196}^-\text{CD183}^-\text{CD194}^+$, and Treg as $\text{CD25}^+\text{FoxP3}^+$ [37].

2.13. Analysis of monocyte differentiation toward antigen-presenting cells

To induce dendritic cell (DC) differentiation, 2.5×10^5 PBMC were cultured in 48-well plates for four days (Corning) in the presence of 50 ng/mL recombinant human IL-4 (R&D Systems, Minneapolis, MN, USA) and 50 ng/mL granulocyte macrophage colony stimulating (GM-CSF, Miltenyi Biotec) in 0.5 mL RPMI 1640 complete medium (Sigma Aldrich). Complete maturation was reached by adding 0.1 $\mu\text{g}/\text{mL}$ lipopolysaccharide (LPS, Sigma Aldrich) for two days.

Monocyte-derived M1 macrophages were obtained from 5×10^5 PBMCs cultured in 24-well plates for four days (Corning) in the presence of 5 ng/mL GM-CSF (Miltenyi Biotec) in 0.5 mL of RPMI 1640 complete medium (Sigma Aldrich). Cells were fully differentiated to M1 macrophages by exogenously administering 20 ng/mL interferon gamma (IFN- γ) for 1 h, followed by 0.1 $\mu\text{g}/\text{mL}$ LPS (Sigma-Aldrich) and incubated for two days.

M1 differentiation was assessed by flow cytometry analysis. Cells were stained with E-Fluor 780 (ThermoFisher) to exclude dead cells and only live cells were analyzed. The gating strategy is the following: live cells gated as negative for CD3 expression were subsequently analyzed for the expression of CD11b (clone ICRF44). CD11b positive cells were then examined for the expression of CD163 (clone GHI/61), CD209 (clone DCN46), CD197 (clone 3D12), CD86 (clone 2331(FUN-1)), and CD14 (clone MP9) (all antibodies were purchased from BD Biosciences).

2.14. Statistical analysis

For tests on PBMC, the data are represented as violin truncated plots with Tukey variations. The parameters were compared using two-way analysis of variance (ANOVA). Data are representative of at least three independent experiments. Statistical analysis was performed using Prism 8 (GraphPad Software). For all tests on cancer cell lines, one-way ANOVA and Turkey post-hoc test was used. A p value lower than 0.05 was considered statistically significant.

3. Results and discussion

3.1. Characterization of PLGA-GO scaffolds

PLGA-GO scaffolds were 3D printed via an extrusion-based and characterized by atomic force microscopy (AFM) to inspect surface topology and roughness, and by Fourier-transform infrared spectroscopy (FTIR) to confirm the chemical composition of the materials. Results are reported in Fig. 1. Scaffolds with a diameter of 12 mm were 3D printed having different concentrations of GO: 0, 0.5, 1, 2 and 5% w/w (Fig. 1A). AFM imaging depicted a sharply different surface topology between PLGA and PLGA-GO scaffolds (Fig. 1B), highlighting a GO concentration-dependent increase in the surface roughness both in terms of arithmetic average of profile height deviations from the mean line, Ra, and root mean square average of profile height deviations from the mean line, Rq (Fig. 1C). FTIR analysis is reported on Fig. 1D for PLGA and E for PLGA-GO scaffolds. Both spectra showed typical absorption peaks at 2990 and 2890 cm^{-1} , corresponding to the C–H stretch of CH_2 , and of –C–H– respectively [38]. Moreover, both scaffolds had a peak at 1700 cm^{-1} and a peak at 1000 cm^{-1} , corresponding to the C=O stretching of the ester bond and to the C–O respectively [39]. Interestingly, the presence of GO within the 3D printed materials was confirmed on PLGA-GO spectra by highlighting a broad absorption peak ranging from 3600 to 3100 cm^{-1} , which corresponds to the O–H stretching vibration, and a narrower peak at 1500 cm^{-1} , corresponding to the C=O bond [40,41]. After microscopic and spectroscopic characterization, PLGA-GO scaffolds were tested to perform PTT/PDT. For this purpose, scaffolds were placed on a 48-well plate and immersed in culture medium. 3D printed materials were then irradiated with an 808 nm infrared laser at different power densities, to achieve the same thermal increase regardless the concentration of GO. The laser was first characterized by recording its power with respect to the current (Fig. 1F). NIR radiation was exerted investigating the most effective and efficient approach for administering photothermal/photodynamic radiation as an anticancer therapy. In this study, we compared two distinct photothermal strategies: a single radiation lasting 9 min, namely NF, and a fractionated approach comprising three radiations of 3 min each, administered consecutively over three days (namely t1, t2 and t3). Power densities used for NIR radiation on each scaffold are reported in Fig. 1G. 3D printed PLGA was irradiated with the highest tested power density, expecting no thermal increase over time due to the absence of photoabsorbers within the scaffold. Temperature increase was monitored for both t3 and NF (Fig. 1H and I respectively). All scaffolds reached the same temperature in both timespans, regardless the different concentrations of GO. PLGA scaffolds without GO did not achieve a significant temperature raise in both therapeutic strategies. We then investigated the NIR radiation photodynamic effect on bare scaffolds. Our findings reveal a statistically significant increase in the production of reactive oxygen species (ROS, Fig. 1J) and superoxide (O_2^\bullet , Fig. 1K) following scaffold irradiation. Notably, the discrimination between general ROS and superoxide was achieved through the use of two distinct probes: a green fluorescent dye for the detection of general ROS, such as hydrogen peroxide (H_2O_2), peroxyxynitrite (ONOO^-), hydroxyl radicals (OH^\bullet), nitric oxide (NO), and peroxy radical (ROO); an orange fluorescent probe, capable of detecting O_2^\bullet . This emphasizes the critical importance of evaluating the PDT potential of such constructs, shedding light on their ability to selectively generate ROS and superoxide upon NIR stimulation. The observed rise in ROS production underscores the efficacy of the designed scaffolds in utilizing light energy for therapeutic applications, underscoring their promise in advancing photothermal and photodynamic treatments.

3.2. Comparison of NF/t3 NIR radiation regimens on PBMC viability

Before investigating the effect of hyperthermia on the immune cell functions, we determined whether the exposure to t3 vs NF irradiation

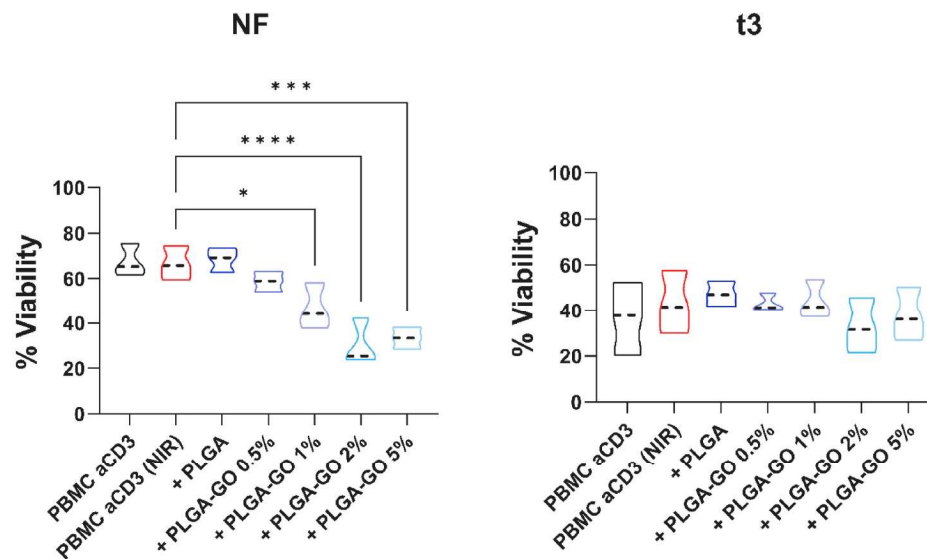


Fig. 2. Impact of hyperthermia regimens on PBMC viability. PBMC were stimulated with anti-CD3 mAb in the presence of PLGA scaffolds conjugated with different concentrations of GO (0.5, 1, 2 and 5%) in comparison to the control condition in red, second lane, at the two different hyperthermia regimens: NF (A, left panel) or t3 (B, right panel). Results are expressed as percentage of viable cells. Results are displayed as violin plots showing median (thick line), 25th and 75th quartiles (* $p < 0.01$, *** $p < 0.001$ versus control (PBMC + anti-CD3), $N \geq 3$ individual experiments).

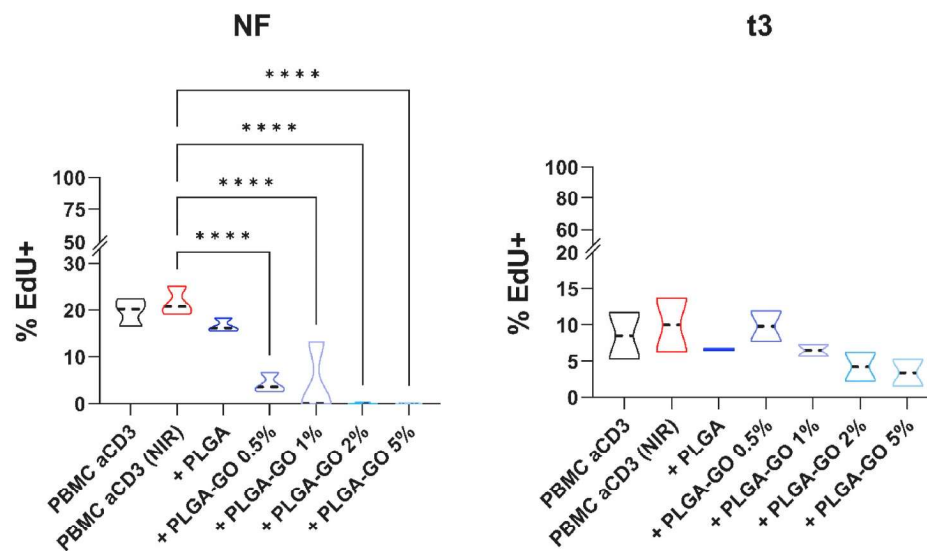


Fig. 3. Impact of hyperthermia regimens on PBMC proliferation. PBMC were stimulated with anti-CD3 mAb in the presence of PLGA scaffolds with different concentrations of GO (0.5, 1, 2 and 5%) in comparison to the control condition in red, second lane, at the two different hyperthermia regimens: NF (A, left panel) or t3 (B, right panel). Results are expressed as percentage of Edu positive proliferating cells. Results are displayed as violin plots showing median (thick line), 25th and 75th quartiles (* $p < 0.01$, *** $p < 0.001$ versus control (PBMC + anti-CD3), A: $N \geq 3$; individual experiments).

by infrared laser differently affected the viability of activated PBMC in the different culture conditions (i.e. in presence/absence of PLGA or PLGA-GO scaffolds). We observed that the laser irradiation applied by the NF protocol induces a strong and progressive cell death; this is also observed in the presence of scaffolds with increasing concentrations of GO. A general reduction in cell viability was observed during the t3 treatment. This effect can be attributed to the experimental conditions, which require daily treatment, for three consecutive days. However, laser irradiation of the t3 protocol had minimal effect on cell viability, even at the highest GO concentrations (Fig. 2B, right panel).

3.3. Comparison of NF/t3 NIR radiation regimens on PBMC proliferation

We next sought to assess the impact of irradiation on PBMC

proliferation in response to stimulation with anti-CD3 mAb. At first, we found that regardless the protocol applied, irradiation did not affect the ability to PBMC to proliferate in response to anti-CD3 stimuli (violin plot red, second lane for both, Fig. 2A–B). Similarly, the presence of PLGA scaffold did not affect the proliferation of activated PBMC. In contrast, in presence of PLGA-GO scaffolds the application of NF irradiation strongly impaired PBMC proliferation even at the lowest concentration of GO; indeed 1, 2% and 5% PLGA-GO completely inhibited the proliferation of PBMC (Fig. 3A, left panel).

On the other hand, we observed that stimulated PBMC respond better to the stress induced by the hyperthermia when applied as t3 protocol, indeed PBMC proliferation was only slightly reduced in presence of PLGA scaffolds having GO at 0.5% and 1%. The higher GO concentrations, 2% and 5%, induced a reduction in PBMC proliferation but